Geochemical Perspectives Letters

Release of subducted sedimentary nitrogen throughout Earth's mantle

P.H. Barry[1,2]*, D.R. Hilton[1]

OPEN ACCESS

Abstract

doi: 10.7185/geochemlet.1615

The dynamic process of subduction represents the principal means to introduce chemical heterogeneities into Earth's interior. In the case of nitrogen (N) - atmosphere's most abundant gas - biological-activity converts N_2 into ammonium ions (NH_4^+), which are chemically-bound within seafloor sediments and altered oceanic crust that comprise the subducting slab. Although some subducted N re-emerges via arc-related volcanism (Sano *et al.*, 1998; Fischer *et al.*, 2002), the majority likely bypasses sub-arc depths (150-200 km) and supplies the deeper mantle (Li *et al.*, 2007; Mitchell *et al.*, 2010; Johnson and Goldblatt, 2015; Bebout *et al.*, 2016). However, the fate of subducted N remains enigmatic: is it incorporated by the shallow convecting mantle - the source of ridge volcanism, or is the deeper mantle - nominally associated with mantle plumes - its ultimate repository? Here, we present N-He-Ne-Ar isotope data for oceanic basalts from the Central Indian Ridge (CIR)-Réunion plume region to address this issue. All on-axis samples with depleted MORB mantle (DMM) affinities ($^3He/^4He$ = 8 ± 1 R_A; Graham, 2002) have low N-isotopes (mean $\delta^{15}N$ = -2.1 ‰), whereas those with plume-like $^3He/^4He$ display higher values (mean $\delta^{15}N$ = 1.3 ‰). We explain these data within the framework of a new mantle reference model to predict a time-integrated net N regassing flux to the mantle of ~3.4 × 10^{10} mol/yr, with the plume-source mantle representing the preferential destination by a factor of 2-3. The model has implications for the present-day imbalance between N subducted at trenches and N emitted via arc-related volcanism, the N-content of Earth's early atmosphere, as well as relationships between N_2 and the noble gases in mantle reservoirs, including $^3He/^4He$-$\delta^{15}N$ relationships in plume-derived lavas.

Received 3 February 2016 | Accepted 11 April 2016 | Published 3 May 2016

Letter

The CIR-Réunion plume system is a classic modern example of oblique plume-ridge interaction, with the present-day plume centred at Réunion Island and three submarine off-ridge segments, the Rodriguez, Three Magi and Gasitao ridges,

1. Fluids & Volatiles Laboratory, Scripps Institution of Oceanography, UC San Diego, La Jolla, California 92093-0244, USA
2. Present address: Department of Earth Sciences, University of Oxford, OX1 3AN, UK

* Corresponding author (email: peter.barry@earth.ox.ac.uk)

connecting with the CIR ridge axis located ~1100 km to the east. These west-to-east trending ridges were formed by volcanism above a channel of Réunion hotspot mantle as the CIR migrated northeast over and away from the plume (Morgan, 1978). He-isotopes – the canonical tracer of mantle plume involvement in petrogenesis – are higher (>9 R_A) than typical DMM values of 8 ± 1 R_A (where R_A = air-like $^3He/^4He$) at Réunion Island and along the off-axis ridges. In contrast, the CIR exhibits DMM-like $^3He/^4He$ values along axis, except at the point where the projection of the submarine ridges meets the ridge axis ~19.9 °S (Füri *et al.*, 2011; Fig. S-1).

New nitrogen isotope and abundance analyses, along with accompanying neon and argon data, of basaltic glasses from the CIR axis between 16.7 °S and 20.6 °S, and from the off-axis ridges to the west of the CIR (Fig. S-1) are presented in Table 1a and b. In addition, we report Ne and Ar isotope and abundance data on olivine separates of a suite of cumulate dunite xenoliths from Réunion Island. Samples were processed by vacuum crushing with released gases analysed using a noble gas mass spectrometer (Barry *et al.*, 2012). All samples have been analysed previously for He isotopes, major/minor and trace element chemistry (Füri *et al.*, 2011).

Nitrogen isotope results are presented in the $\delta^{15}N$ notation (where $\delta^{15}N = ((^{15}N/^{14}N_{sample}/^{15}N/^{14}N_{air})-1) \times 1000$) and plotted against He isotopes in Figure 1a, and displayed in comparison to the $\delta^{15}N$ database of ocean basalts in Figure 1b. We highlight the following key features of the N-isotope results. First, all on-axis samples (with the exception of D9-2; $\delta^{15}N$ = 1.16 ‰) have negative $\delta^{15}N$ values. The highest and lowest values are -0.10 and -3.8 ‰ giving an on-axis $\delta^{15}N$ mean value of -2.1 ± 1.1 ‰ (1σ; n = 7) or -1.7 ± 1.6 ‰ (n = 8 if D9-2 is included). Notably, sample D9-2 has a $^3He/^4He$ ratio (7.25 R_A), which falls in the nominal DMM range (8 ± 1 R_A; Graham, 2002) characteristic of most samples on the CIR ridge-axis (Füri et al., 2011). The only on-axis sample (DR10-1) of the present sample suite with a $^3He/^4He$ value higher than DMM ($^3He/^4He$ = 10.31 R_A) is from the region where the projection of the off-axis ridge impinges the spreading centre (~19.9 °S): it has a $\delta^{15}N$ value of -0.10 ‰ – the second highest value of the on-axis samples. Second, the three off-axis samples – all with $^3He/^4He$ > 9 R_A – have positive $\delta^{15}N$ values, ranging from +0.89 to +1.80 ‰; with a mean value of 1.3 ± 0.7 ‰ (1σ). Thus, with the exception of sample D9-2, there is a clear distinction between relatively low $\delta^{15}N$ values associated with DMM-like He-isotopes on the ridge axis and relatively high $\delta^{15}N$ values associated with plume-like $^3He/^4He$ values off-axis. Finally, we point out that with the exception of sample D8-2, all $\delta^{15}N$ values, irrespective of location on- or off-axis, are higher than the range nominally associated with DMM ($\delta^{15}N$ = -5 ± 2 ‰; Fig. 1b). Thus, samples of this study have experienced enrichment in ^{15}N compared to the majority of basalts erupted at ridge axes worldwide.

There are three processes capable of producing high (>DMM) $\delta^{15}N$ signatures in CIR basalts: (1) assimilation of existing crust during magma eruption, likely also involving incorporation of air ($\delta^{15}N$ = 0 ‰), (2) mass-dependent

Table 1a Neon and argon isotope systematics of submarine basaltic glasses from the CIR (on-axis) and adjacent (off-axis) Gasitao Ridge, Three Magi Ridges and Abyssal Hill, and olivine separates from dunite xenoliths of Piton Chisny (Réunion).

Sample	$^{20}Ne/^{22}Ne$	$^{21}Ne/^{22}Ne$	$^{20}Ne \times 10^{-9}$ cm^3 STP/g	$^{40}Ar/^{36}Ar$	$[^{40}Ar] \times 10^{-9}$ cm^{3}STP/g
On-Axis					
D1-1	10.10 ± 0.11	0.0316 ± 0.0003	0.67 ± 0.012	290.6 ± 0.1	2416 ± 0.3
D1-1 (Dup)	-	-	-	-	-
D3-1	9.90 ± 0.10	0.0291 ± 0.0001	2.28 ± 0.025	296.1 ± 0.3	765 ± 0.5
D2-1	9.85 ± 0.10	0.0295 ± 0.0003	2.21 ± 0.030	349.4 ± 0.3	1415 ± 0.9
D8-2	9.93 ± 0.10	0.0302 ± 0.0002	0.76 ± 0.017	3520 ± 12	724 ± 0.2
D9-2	-	-	-	-	-
D15-1	10.34 ± 0.11	0.0327 ± 0.0004	0.55 ± 0.008	2193 ± 3.3	1968 ± 2.6
D14-1	10.34 ± 0.12	0.0324 ± 0.0008	0.25 ± 0.019	2413 ± 5.8	1326 ± 0.3
D14-1 (Dup)	10.43 ± 0.11	0.0331 ± 0.0004	0.25 ± 0.012	1514 ± 3.9	761 ± 0.7
DR10-1					
D13-1	10.72 ± 0.12	0.0340 ± 0.0006	0.20 ± 0.023	3519 ± 12	722 ± 0.2
D13-1 (Dup)	11.32 ± 0.13	0.0401 ± 0.0007	0.10 ± 0.004	8487 ± 43	1272 ± 0.5
Off-Axis ***Three Magi Ridges***					
D22-1	9.89 ± 0.10	0.0296 ± 0.0002	1.89 ± 0.011	408.5 ± 0.6	1903 ± 0.8
D22-1 (Dup #1)	-	-	-	-	-
D22-1 (Dup #2)	-	-	-	-	-
D26-2	9.87 ± 0.10	0.0296 ± 0.0002	1.15 ± 0.025	554.6 ± 0.5	1268 ± 0.9
Gasitao Ridge					
D20-5	9.84 ± 0.23	0.0294 ± 0.0013	0.17 ± 0.020	1725 ± 12	421 ± 0.1
D20-5 (Dup #1)	10.05 ± 0.13	0.0304 ± 0.0009	0.12 ± 0.007	1786 ± 4.8	383 ± 0.1
D20-5 (Dup #2)	10.05 ± 0.12	0.0317 ± 0.0010	0.14 ± 0.013	1576 ± 5.2	401 ± 0.3
D18-1	9.89 ± 0.11	0.0290 ± 0.0004	0.14 ± 0.006	396.1 ± 3.0	16 ± 0.1
Abyssal Hill					
D37-2	9.86 ± 0.10	0.0294 ± 0.0001	1.19 ± 0.022	318.4 ± 0.4	849 ± 0.7
Réunion Island					
CH07-01	10.49 ± 0.11	0.0306 ± 0.0005	0.30 ± 0.006	1294 ± 3.0	776 ± 0.2
CH07-02	10.00 ± 0.11	0.0296 ± 0.0004	0.33 ± 0.007	501.2 ± 1.0	327 ± 0.2
CH07-04	10.09 ± 0.12	0.0314 ± 0.0014	0.06 ± 0.007	705.1 ± 3.5	125 ± 0.1
CH07-07	10.26 ± 0.11	0.0296 ± 0.0008	0.20 ± 0.006	831.3 ± 2.0	308 ± 0.1

Table 1b Nitrogen and He isotope systematics, and relative He-N-Ar abundances of submarine basaltic glasses from the CIR (on-axis) and adjacent (off-axis) Gasitao Ridge, Three Magi Ridges and Abyssal Hill, and olivine separates from dunite xenoliths of Piton Chisny (Réunion).

Sample	$[N_2] \times 10^{-6}$cm^3 STP/g[a]	$\delta^{15}N$ (‰)[b]	N_2/Ar[c]	$^3He/^4He$ (R/R_A)[d]	$^4He/^{40}Ar^*$
On-Axis					
D1-1	5.56	-1.93 ± 0.91	132	8.11 ± 0.11	-
D1-1 (Dup)	5.21	-1.25 ± 0.71	99.9	-	-
D3-1	4.97	-1.81 ± 1.13	68.5	7.91 ± 0.02	-
D2-1	-	-	-	8.19 ± 0.09	62 ± 0.2
D8-2	21.1	-3.81 ± 0.51	156	7.08 ± 0.14	7.5 ± 0.9
D9-2	10.5	1.16 ± 0.59	267	7.25 ± 0.08	-
D15-1	38.7	-2.34 ± 0.55	281	8.68 ± 0.01	8.4 ± 0.3
D14-1	16.0	-2.01 ± 0.38	238	8.46 ± 0.02	6.9 ± 0.4
D14-1 (Dup)	-	-	-	-	10 ± 0.4
DR10-1	48.0	-0.10 ± 0.63	47.9	10.31 ± 0.06	-
D13-1	20.9	-1.99 ± 0.53	85.6	8.26 ± 0.03	3.0 ± 0.1
D13-1 (Dup)	14.1	-2.68 ± 0.51	131	-	6.0 ± 2.6
Off-Axis ***Three Magi Ridges***					
D22-1	74.2	1.71 ± 0.45	82.8	9.40 ± 0.06	23 ± 0.1
D22-1 (Dup #1)	78.7	1.80 ± 0.52	127	-	-
D22-1 (Dup #2)	92.6	1.74 ± 0.48	104	-	-
D26-2	15.2	0.89 ± 0.83	129	9.51 ± 0.02	5.2 ± 0.1
Gasitao Ridge					
D20-5	-	-	-	8.28 ± 0.05	11 ± 1.3
D20-5 (Dup #1)	-	-	-	-	9.3 ± 0.4
D20-5 (Dup #2)	-	-	-	-	11 ± 0.6
D18-1	2.34	1.14 ± 1.47	244	9.09 ± 0.06	31 ± 0.9
Abyssal Hill					
D37-2	-	-	-	9.67 ± 0.17	18 ± 0.1
Réunion Island					
CH07-01	-	-	-	13.95 ± 0.25	1.3 ± 0.1
CH07-02	-	-	-	13.66 ± 0.22	1.5 ± 0.1
CH07-04	-	-	-	14.09 ± 0.23	2.0 ± 0.1
CH07-07	-	-	-	13.58 ± 0.15	1.5 ± 0.1

[a] N_2 concentration measurements are accurate within 3 %, based on the reproducibility of standards.
[b] Uncertainties on $\delta^{15}N$ are 1σ. Blank subtractions and a comprehensive CO correction have been applied to all $\delta^{15}N$ results.
[c] All N_2/Ar uncertainties are less than 10 %. Blank subtractions have been applied to all N_2/Ar results.
[d] Data previously reported in Füri *et al.*, 2011.

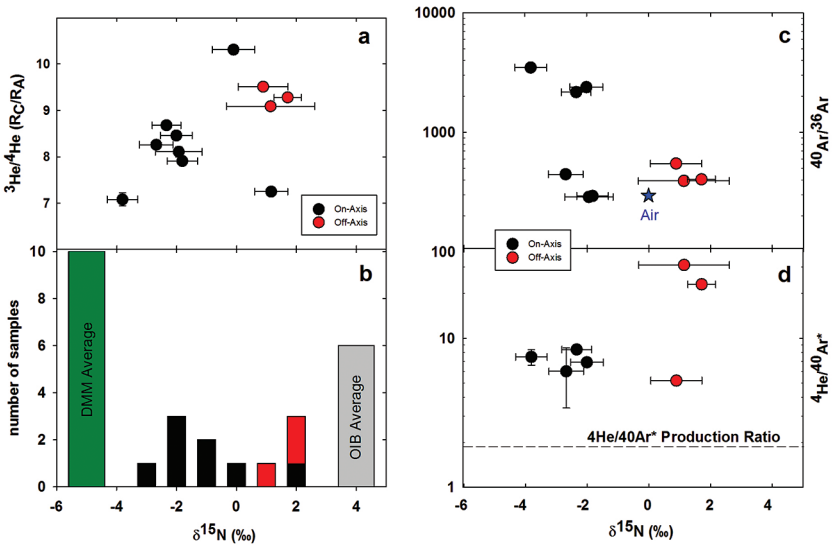

Figure 1 **(a)** He-isotopes (^{3}He/^{4}He) versus N-isotopes, showing high (positive) δ^{15}N values in all off-axis samples with >DMM-like ^{3}He/^{4}He values. **(b)** Histogram of N-isotopes measured along the CIR (in black) and its adjacent ridges (in red) relative to global DMM (green) and OIB (grey) averages (from Cartigny and Marty, 2013). **(c)** Argon isotopes (^{40}Ar/^{36}Ar) versus N-isotopes. **(d)** ^{4}He/^{40}Ar* (degassing proxy) versus N-isotopes suggests that high δ^{15}N values are not produced by magmatic degassing (see text).

fractionation related to magmatic degassing (Cartigny *et al.*, 2001), and/or (3) recycling of oceanic sediments and/or oceanic crust (δ^{15}N ~+5 to +7 ‰) into the CIR mantle source region producing the melts (Marty and Dauphas, 2003). The latter possibility implies that δ^{15}N is a feature intrinsic to the mantle source, whereas the former two are predominantly shallow-level phenomena that act to mask primary (source) δ^{15}N signatures.

There is little evidence in either the on- or off-axis N database (Table 1a and b) for a correlation between high N-contents – possibly reflecting crustal assimilation and/or air addition – and high δ^{15}N values. For example, there is a 30-fold difference in N-content between off-axis samples D22-1 and D18-1 yet they have indistinguishable δ^{15}N values. Similarly, two of the three highest N-content on-axis samples (D8-2 and D15-1) have the lowest δ^{15}N values of this suite. Both observations are inconsistent with addition of air and/or crustal N, which would act to increase both δ^{15}N and N-content of samples. Furthermore, a plot of ^{40}Ar/^{36}Ar versus δ^{15}N (Fig. 1c) shows no correlation for either on- or off-axis samples: all on-axis samples fall within 2σ of the mean value of -2.1 ‰, yet ^{40}Ar/^{36}Ar values range between 8500 and close to the atmospheric value (298.6; Lee *et al.*, 2006), *i.e.* samples with low ^{40}Ar/^{36}Ar values do not have δ^{15}N values closer to air (0 ‰). Finally, off-axis samples are characterised by markedly

different ^{4}He/^{40}Ar* ratios – a parameter sensitive to magma degassing due to the factor of ~10 difference in solubility between He and Ar in basaltic melt (Lux, 1987). Although ^{4}He/^{40}Ar* ratios vary between 5-31 for samples D18-1 and D26-2, respectively, their δ^{15}N values are virtually identical at 1.14 and 0.89 ‰ (Fig. 1d). Thus, we conclude that the range in δ^{15}N values reported here reflects intrinsic mantle source features, likely related to subduction of ^{15}N-enriched oceanic sediments and/or oceanic crust.

The neon isotope characteristics of CIR lavas are plotted on a traditional three-isotope Ne diagram (Fig. S-2). We note that all samples lie intermediate to air-DMM and air-Réunion mixing trajectories with no clear distinction between on- and off-axis samples. Thus, all CIR basalts comprise three Ne components: air, a primitive/solar (mantle) Ne component and in-situ nucleogenic ^{21}Ne, which has in-grown over time. We subtract the air-derived Ne to yield a mantle ^{21}Ne/^{22}Ne ratio (the so-called extrapolated value – (^{21}Ne/^{22}Ne$_{EX}$); see Supplementary Information for details). This approach allows us to assess mantle neon features of both on- and off-axis samples without compromise of air contamination, and to compare Ne isotopes to corresponding N-isotope variations.

In Figure 2, we plot the extrapolated Ne-isotope values (^{21}Ne/^{22}Ne$_{EX}$) of all basalts against measured δ^{15}N together with endmember compositions for (1) pre-solar nitrogen (PSN), (2) depleted MORB mantle (DMM) and (3) sediment-modified mantle (SMM). Pure DMM has a δ^{15}N value of ~-5 ± 2 ‰, which reflects mixing between N incorporated at the time of planetary accretion – small amounts of primordial N (δ^{15}N <-40 ‰), possibly as low as proto-solar-nebula (PSN) nitrogen (δ^{15}N = -383 ± 8 ‰), and nitrogen introduced into the mantle by long-term recycling of atmospheric (= 0 ‰) and/or sediment-derived (= ~+5 to +7 ‰) components (Marty, 2012). SMM nitrogen reflects superimposition and dominance of recently-added sedimentary N relative to pure DMM, as observed at convergent margins such as Costa Rica (Fischer *et al.*, 2002). For Ne-isotopes, a DMM ^{21}Ne/^{22}Ne endmember value (0.0594) is derived by extrapolating the MORB trajectory (Sarda *et al.*, 1988) to the ^{20}Ne/^{22}Ne value of Ne-B (= 12.5) and noting the ^{21}Ne/^{22}Ne value at that point. Solar Ne is defined by the solar wind value of 0.03118 (Trieloff and Kunz, 2005). We assume that subduction of oceanic sediments and crust does not introduce neon (or helium) into the mantle (Hilton *et al.*, 1992) so that DMM and SMM have the same ^{21}Ne/^{22}Ne$_{EX}$ value.

The coupled δ^{15}N-^{21}Ne/^{22}Ne$_{EX}$ characteristics of both sets of basaltic glasses (*i.e.* on- and off-axis) are compatible with mixing between two distinct endmember compositions (Fig. 2). One endmember, with low δ^{15}N and low ^{21}Ne/^{22}Ne$_{EX}$, is common to both sample suites, with solar gas being the most plausible candidate. In contrast, the second endmember differs between on- and off-axis samples. In the case of CIR on-axis basalts, the endmember has a DMM ^{21}Ne/^{22}Ne$_{EX}$ value (0.060) and δ^{15}N = -2.1 ‰ whereas the off-axis samples project to an endmember with a higher δ^{15}N (~1.3 ‰) but the same DMM-like ^{21}Ne/^{22}Ne$_{EX}$ value. Notably, both on- and off-axis endmembers lie on the projection between pure DMM and SMM with the proportion of N derived from SMM clearly greater in off-axis samples versus on-axis samples (Fig. 2).

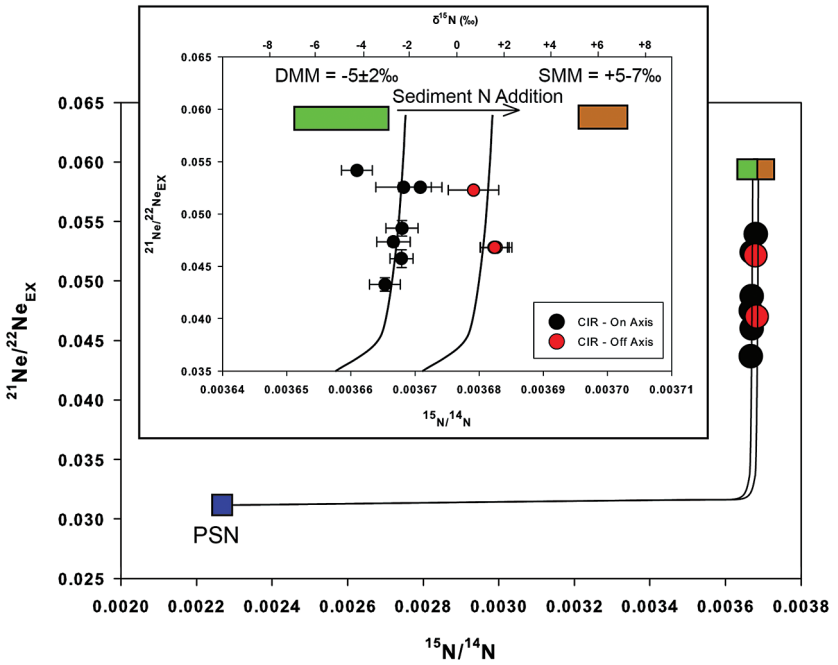

Figure 2 Extrapolated Ne ($(^{21}Ne/^{22}Ne)_{EX}$, *i.e.* air-corrected $^{21}Ne/^{22}Ne$ values) versus $^{15}N/^{14}N$ values of CIR basalts, plotted together with binary mixing curves between a pre-solar nitrogen (PSN) component ($^{15}N/^{14}N$ = 0.00227, $\delta^{15}N$ = -373 ‰; Marty, 2012) and two mantle endmember components reflecting addition of ^{15}N-enriched sedimentary MORB mantle (SMM; $\delta^{15}N$ = +5 ‰) to DMM mantle ($\delta^{15}N$ = -5 ‰). The curvature of the hyperbolic mixing lines is described by the r-value = $(^{14}N/^{22}Ne)_{DMM/SMM}/(^{14}N/^{22}Ne)_{PSN}$.

The curvature of the binary mixing trajectories in Figure 2 has important implications for the overall recycling efficiency of N relative to Ne, as it is controlled by the relative $^{14}N/^{22}Ne$ ratios of the two endmembers (r-value). For both on- and off-axis samples, r ≥ 1000, which indicates either higher relative ^{14}N or lower ^{22}Ne contents in the mixed DMM-SMM versus the PSN endmember: this indicates that N is recycled at least 10^3 times more efficiently than Ne into the CIR mantle. Preferential deep recycling of N relative to Ne is consistent with recent theoretical and experimental predictions that indicate that N is stabilised as ammonium under subduction redox conditions (fO_2 < QFM; Mikhail and Sverjensky, 2014) and therefore behaves as a large ion lithophile element whereby it can substitute into K-bearing silicate minerals and gain stability in the downgoing slab (Li *et al.*, 2013). Moreover, mass balance arguments suggest Ne is efficiently recycled back to the surface during the subduction process (Holland and Ballentine, 2006; Marty, 2012).

The CIR data reaffirms the considerable heterogeneity in mantle $\delta^{15}N$ signatures (*e.g.*, Marty and Dauphas, 2003). If we assume that on-axis samples can be used to approximate the N composition of the DMM and that off-axis samples best represent the plume mantle (PLM), then CIR data can be used within the framework of a newly-constructed reference model to place constraints on N regassing fluxes into the mantle (*i.e.* both absolute flux values as well as the relative proportions regassing the DMM and PLM reservoirs). Our model is based on a layered mantle reservoir concept, similar to that described for noble gases by O'Nions and Tolstikhin (1996) and Gonnermann and Mukhopadhyay (2009). It makes the following assumptions: (1) the N regassing flux commences at the onset of subduction and is constant through time; (2) a constant proportion of the total N regassing flux (F) is subducted into each respective mantle reservoir (defined here as F_{DMM} and F_{PLM}) and instantaneously mixes in each reservoir; (3) there is a constant mantle degassing flux of 5×10^9 mol/yr (Cartigny and Marty, 2013), derived from the DMM:PLM reservoirs in the proportion 85:15, respectively (Ito *et al.*, 2003); (4) the present-day mantle N-content ([N]) is ~0.27 ± 0.16 ppm (Marty, 2012; Cartigny and Marty, 2013); and (5) the initial mantle $\delta^{15}N$ is -40 ‰ (PSN-like; Cartigny and Marty, 2013) which is unmodified by any degassing prior to the onset of subduction. The DMM and PLM reservoirs are considered to have evolved to their current $\delta^{15}N$ and [N] compositions, given by the CIR data, as a consequence of additions of different amounts of subducted sedimentary N ($\delta^{15}N$ = +5 ‰).

A DMM mass of ~9×10^{26} g (*e.g.*, Anderson, 1989) corresponds to a total inventory of 17.3×10^{18} mol N in the modern-day DMM. Assuming that the mantle degassing flux (5×10^9 mol/yr; Cartigny and Marty, 2013) includes all non-arc related N (*i.e.* N degassed from the mantle) and is 85 % DMM-derived (4.3×10^9 mol/yr) and 15 % plume mantle-derived (7.5×10^8 mol/yr), then a total of 10.6×10^{18} mol N has been degassed from the DMM source over an estimated 2.5 Ga since subduction commenced (*e.g.*, Kusky *et al.*, 2001). For a total N-content of 27.9×10^{18} mol N before degassing, the present-day N-isotopic composition of -2.1 ‰ must represent admixture between 23.5×10^{18} moles of subduction-derived N ($\delta^{15}N$ = +5 ‰), or ~84 % of the total N, and 4.4×10^{18} moles (or 16 %) of PSN ($\delta^{15}N$ = -40 ‰). Thus, the time integrated DMM regassing rate (F_{DMM}) is 9.4 x 10^9 moles/yr.

Using the same approach for the PLM – assumed to be represented by off-axis high $^3He/^4He$ plume melts with an average $\delta^{15}N$ = 1.3 ‰, then a mass of ~3.3×10^{27} g would contain 64×10^{18} mol N in the modern day plume-influenced mantle. Again assuming a constant mantle degassing flux of 5×10^9 mol/yr (Cartigny and Marty, 2013), of which ~15 % (*i.e.* 7.5×10^8 mol/yr) is derived from this reservoir (Ito *et al.*, 2003), then a total of 1.9×10^{18} mol N has been degassed from the plume-influenced mantle over 2.5 Ga. The total N-content of 65.9×10^{18} mol requires 61×10^{18} moles N (~92 % of the total) of subduction-derived N ($\delta^{15}N$ = +5 ‰) mixing with 8 % (*i.e.* 5.4×10^{18} moles) of PSN ($\delta^{15}N$ = -40 ‰) to give the present-day N-isotopic composition of 1.3 ‰. Thus, the model predicts a regassing N-flux (F_{PLM}) of ~2.4×10^{10} mol/yr since the Archean (2.5 Ga). Importantly,

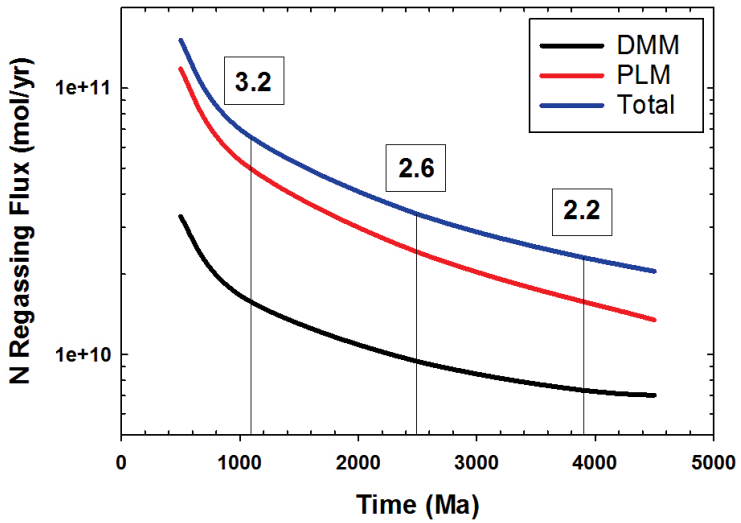

Figure 3 Nitrogen regassing fluxes (mol/yr) into the mantle as a function of time (Ma) since the onset of subduction. The total flux is equal to the sum of DMM and PLM fluxes. The proportion of N regassed into the plume-influenced mantle relative to the DMM (F_{PLM}/F_{DMM}) is shown in boxes at three given time intervals (1.1 Ga, 2.5 Ga, 3.9 Ga).

in order to satisfy the N systematics for both reservoirs, approximately 2.6 times more N (*i.e.* F_{PLM}/F_{DMM}) must be subducted into the plume-influenced mantle. If subduction is assumed to have initiated earlier in the geological record (*e.g.*, 3.9 Ga; Condie and Pease, 2008), then the F_{PLM}/F_{DMM} ratio decreases to ~2.2. Conversely, if an estimated modern day N input flux of 7×10^{10} mol/yr (Cartigny and Marty, 2013) is adopted, it would take the Earth only 1.1 Ga to evolve to its current N composition, with $F_{PLM}/F_{DMM} = 3.2$ (Fig. 3; Table S-1).

Selection of different $\delta^{15}N$ endmembers for mantle reservoirs or lower initial solar values as input parameters has only a minor effect on model results (Table S-1). If more extreme N-isotope estimates of -4 ‰ and +3 ‰ are taken to approximate DMM and PLM sources, respectively (Dauphas and Marty, 1999), then an identical PLM regassing flux of 2.4×10^{10} mol/yr is calculated for 2.5 Ga with only a marginally higher $F_{PLM}/F_{DMM} = 2.8$. Alternatively, a significantly higher estimate for the mantle N-content of ~36 ppm (Cartigny and Marty, 2013) results in a 2.5 Ga regassing flux of 3.9×10^{12} mol/yr with a $F_{PLM}/F_{DMM} = 4$. Significantly, all model scenarios point to long-term cycling of subducted N into Earth's mantle with preferential storage in the deep (plume) mantle (*i.e.* $F_{PLM}/F_{DMM} > 2$). Thus nitrogen not only breaches the subduction barrier beneath arcs but is also transported into the (deep mantle) source region that supplies high $^3He/^4He$ mantle plumes.

Our new reference model has a number of far-reaching implications. First, given the high N recycling efficiencies into DMM (84 %) and PLM (92 %) reservoirs, respectively (this work), any losses of slab-derived N to the atmosphere at volcanic arcs (*e.g.*, by oxidation back to molecular form in the mantle wedge) must be relatively minor. Thus, our model can explain the present-day gross imbalance between the regassing N flux subducted via trenches and the degassing N flux returned to the surface via arc-related volcanism (Hilton *et al.*, 2002; Busigny *et al.*, 2011). Second, prior to initiation of subduction-related recycling of N, the total N content of the atmosphere must have been considerably higher. Our model indicates that the early atmospheric N content was ~2.1 x 10^{20} moles, or ~50 % higher than at the present-day. Such a high atmospheric N-content would lead to N-enhanced greenhouse warming, and can explain the lack of global glaciations in the early Earth due to the faint young Sun (Goldblatt *et al.*, 2009). Third, subduction of sedimentary N into the deep mantle would lead to a close relationship between high $\delta^{15}N$ values and high $^3He/^4He$ ratios, the canonical geochemical tracer of deep mantle plumes. Recent work on hyaloclastic basaltic glasses in Iceland (Halldórsson *et al.*, 2016) reveals a strong coupling between $^3He/^4He$ and $\delta^{15}N$ signatures, consistent with recycling of crustal material to the mantle plume source. Finally, we highlight remarkably similar recycling efficiencies between N (84-92 %; this work) and heavy noble gases (73-87 %; Holland and Ballentine, 2006; Parai and Mukhopadhyay, 2012) despite fundamentally different subduction mechanisms: N is fixed as NH_4^+ and bound in recycled sediments and/or oceanic crust, whereas Kr and Xe undergo no such chemical transformation and instead are simply dissolved in pore fluids and/or in unoccupied amphibole A-sites within subducted oceanic crust (*e.g.*, Holland and Ballentine, 2006; Jackson *et al.*, 2015).

Acknowledgements

This work was supported by NSF grants EAR-0651097 and OCE-0726573. The KNOX11RR cruise was funded by UC Ship Funds. We thank Sami Mikhail, Ben Johnson and anonymous reviewers for their constructive and insightful comments, and Graham Pearson for editorial handling.

Editor: Graham Pearson

Additional Information

Supplementary Information accompanies this letter at www.geochemicalperspectivesletters.org/article1615

Reprints and permission information is available online at http://www.geochemicalperspectivesletters.org/copyright-and-permissions

Cite this letter as: Barry, P.H., Hilton, D.R. (2016) Release of subducted sedimentary nitrogen throughout Earth's mantle. *Geochem. Persp. Let.* 2, 148-159.

References

Anderson, D.L. (1989) Theory of the Earth. Blackwell Scientific Publications, Boston, http://resolver.caltech.edu/CaltechBOOK:1989.001.

Barry, P.H., Hilton, D.R., Halldórsson, S.A., Hahm, D., Marti, K. (2012) High precision nitrogen isotope measurements in oceanic basalts using a static triple collection noble gas mass spectrometer. *Geochemistry Geophysics Geosystems* 13, Q01019.

Bebout, G.E., Lazzeri, K.E., Geiger, C.A. (2016) Pathways for nitrogen cycling in Earth's crust and upper mantle: A review and new results for microporous beryl and cordierite. *American Mineralogist* 101, 7-24.

Busigny, V., Cartigny, P., Philippot, P. (2011) Nitrogen isotopes in ophiolitic metagabbros: A re-evaluation of modern nitrogen fluxes in subduction zones and implication for the early Earth atmosphere. *Geochimica et Cosmochimica Acta* 75, 7502–7521.

Cartigny, P., Marty, B. (2013) Nitrogen isotopes and mantle geodynamics: The emergence of life and the atmosphere–crust–mantle connection. *Elements* 9, 359-366.

Cartigny, P., Harris, J.W., Javoy, M. (2001) Diamond genesis, mantle fractionations and mantle nitrogen content: a study of δ13 C–N concentrations in diamonds. *Earth and Planetary Science Letters* 185, 85-98.

Condie, K.C., Pease, V. (2008) When did plate tectonics begin on planet Earth? Geological Society of America Special Paper 440, Boulder Colorado, USA.

Dauphas, N., Marty, B. (1999) Heavy nitrogen in carbonatites of the Kola Peninsula: A possible signature of the deep mantle. *Science* 286, 2488-2490.

Fischer, T.P., Hilton, D.R., Zimmer, M.M., Shaw, A.M., Sharp, Z.D., Walker, J.A. (2002) Subduction and recycling of nitrogen along the Central American margin. *Science* 297, 1154-1157.

Füri, E., Hilton, D.R., Murton, B.J., Hemond, C., Dyment, J., Day, J.M.D. (2011) Helium isotope variations between Réunion Island and the Central Indian Ridge (17°-21°S): new evidence for ridge-hotspot interaction. *Journal of Geophysical Research – Solid Earth* 116, B02207.

Graham, D.W. (2002) Noble gas isotope geochemistry of mid-ocean ridge and ocean island basalts: Characterization of mantle source reservoirs. *RIMS* 47, 247-317.

Goldblatt, C., Claire, M.W., Lenton, T.M., Matthews, A.J., Watson, A.J., Zahnle, K.J. (2009) Nitrogen-enhanced greenhouse warming on early Earth. *Nature Geoscience* 2, 891-896.

Gonnermann, H.M., Mukhopadhyay, S. (2009) Preserving noble gases in a convecting mantle. *Nature* 459, 560-563.

Halldórsson, S.A., Hilton, D.R., Barry, P.H., Füri, E., Gronvold, K. (2016) Recycling of crustal material by the Iceland mantle plume: New evidence from nitrogen elemental and isotope systematics of subglacial basalts. *Geochimica et Cosmochimica Acta* 176, 206-226.

Hilton, D.R., Hoogewerff, J.A., Van Bergen, M.J., Hammerschmidt, K. (1992) Mapping magma sources in the east Sunda-Banda arcs, Indonesia: constraints from helium isotopes. *Geochimica et Cosmochimica Acta* 56, 851-859.

Hilton, D.R., Fischer, T.P., Marty, B. (2002) Noble gases and volatile recycling at subduction zones. *Reviews in Mineralogy and Geochemistry* 47, 319-370.

Holland, G., Ballentine, C.J. (2006) Seawater subduction controls the heavy noble gas composition of the mantle. *Nature* 441, 186-191.

Ito, G., Lin, J., Graham, D. (2003) Observational and theoretical studies of the dynamics of mantle plume–mid-ocean ridge interaction. *Reviews of Geophysics* 41, 4.

Jackson, C.R., Parman, S.W., Kelley, S.P., Cooper, R.F. (2015) Light noble gas dissolution into ring structure-bearing materials and lattice influences on noble gas recycling. *Geochimica et Cosmochimica Acta* 159, 1-15.

Johnson, B., Goldblatt, C. (2015) The nitrogen budget of Earth. *Earth-Science Reviews* 148, 150-173.

Kusky, T.M., Li, J.H., Tucker, R.D. (2001) The Archean Dongwanzi ophiolite complex, North China Craton: 2.505-billion-year-old oceanic crust and mantle. *Science* 292, 1142-1145.

Lee, J.Y., Marti, K., Severinghaus, J.P., Kawamura, K., Yoo, H.S., Lee, J.B., Kim, J.S. (2006) A redetermination of the isotopic abundances of atmospheric Ar. *Geochimica et Cosmochimica Acta* 70, 4507-4512.

Li, L., Bebout, G.E., Idleman, B.D. (2007) Nitrogen concentration and δ 15 N of altered oceanic crust obtained on ODP Legs 129 and 185: insights into alteration-related nitrogen enrichment and the nitrogen subduction budget. *Geochimica et Cosmochimica Acta* 71, 2344-2360.

Li, Y., Wiedenbeck, M., Shcheka, S., Keppler, H. (2013) Nitrogen solubility in upper mantle minerals. *Earth and Planetary Science Letters* 377, 311-323.

Lux, G. (1987) The behavior of noble gases in silicate liquids: Solution, diffusion, bubbles and surface effects, with applications to natural samples. *Geochimica et Cosmochimica Acta* 51, 1549-1560.

Marty, B. (2012) The origins and concentrations of water, carbon, nitrogen and noble gases on Earth. *Earth and Planetary Science Letters* 313-314, 56-66.

Marty, B., Dauphas, N. (2003) The nitrogen record of crust-mantle interaction and mantle convection from Archean to present. *Earth and Planetary Science Letters* 206, 397– 410.

Mikhail, S., Sverjensky, D.A. (2014) Nitrogen speciation in upper mantle fluids and the origin of Earth's nitrogen-rich atmosphere. *Nature Geoscience* 7, 816-819.

Mitchell, E.C., Fischer, T.P., Hilton, D.R., Hauri, E.H., Shaw, A.M., De Moor, J.M., Sharp, Z.D., Kazahaya, K. (2010) Nitrogen sources and recycling at subduction zones: Insights from the Izu-Bonin-Mariana arc. Geochemistry, Geophysics, Geosystems 11, 2.

Morgan, W.J. (1978) Rodriguez, Darwin, Amsterdam, a second type of hot spot island. *Journal of Geophysical Research* 83, 5355–5360.

O'Nions, R.K., Tolstikhin, I.N. (1996) Limits on the mass flux between lower and upper mantle and stability of layering. *Earth and Planetary Science Letters* 139, 213-222.

Parai, R., Mukhopadhyay, S. (2012) How large is the subducted water flux? New constraints on mantle regassing rates. *Earth and Planetary Science Letters* 317, 396-406.

Sano, Y., Takahata, N., Nishio, Y., Marty, B. (1998) Nitrogen recycling in subduction zones. *Geophysical Research Letters* 25, 2289-2292.

Sarda, P., Staudacher, T., Allègre, C.J. (1988) Neon isotopes in submarine basalts. *Earth and Planetary Science Letters* 91, 73–88.

Trieloff, M., Kunz, J. (2005) Isotope systematics of noble gases in the Earth's mantle: possible sources of primordial isotopes and implications for mantle structure. *Physics of the Earth and Planetary Interiors* 148, 13-38.